Biomarkers of Neovascular Activity in Age-Related Macular Degeneration Using Oct Angiography

Al-Sheikh, Mayss ; Iafe, Nicholas A ; Phasukkijwatana, Nopasak ; Sadda, SriniVas R ; Sarraf, David

DOI: https://doi.org/10.1097/IAE.0000000000001628

BIOMARKERS OF NEOVASCULAR ACTIVITY IN AGE-RELATED MACULAR DEGENERATION USING OCT ANGIOGRAPHY

MAYSS AL-SHEIKH, MD,*† NICHOLAS A. IAFE, MD,† NOPASAK PHASUKKIJWATANA, MD, PHD,†‡ SRINIVAS R. SADDA, MD,* DAVID SARRAF, MD‡§

Purpose: To study the qualitative and quantitative features of choroidal neovascular (NV) membranes in age-related macular degeneration using optical coherence tomography angiography in patients with active and quiescent NV lesions before and after treatment with anti–vascular endothelial growth factor.

Methods: Macular optical coherence tomography angiography images were obtained using RTVue XR Avanti with AngioVue. Morphologic features and quantitative measurements of the NV lesion were analyzed using en face projection images. The NV lesion was subdivided into inner segment and outer fringe for further fractal dimension analysis.

Results: In a series of 31 eyes, 11 eyes with active NV lesions at baseline and after consecutive follow-up after treatment with anti–vascular endothelial growth factor therapy and 20 eyes with quiescent NV lesions were included in this study. Morphologically, all the quiescent NV lesions versus 63.6% of the active NV lesions demonstrated a prominent central vessel and active leasions demonstrated a greater rate of small vessels branching (82%) and peripheral arcades (82%) than quiescent lesions (30% and 40% respectively) and this was statistically significant. The lesion area and vessel density was not statistically significantly different after treatment or versus quiescent lesions although the latter lesions were reduced in area. Lesion pattern complexity measured by the fractal dimension was statistically significantly lower in the inner part of the lesion after treatment and statistically significantly lower in the total lesion of the quiescent NV compared with the active NV.

Conclusion: Optical coherence tomography angiography is a new, noninvasive imaging modality that can be used to perform qualitative and quantitative analyses of NV lesions. In the future, OCT angiography may provide biomarkers of activity and guide the evaluation and treatment and monitoring of neovascularization in age-related macular degeneration.

RETINA 0:1–11, 2017

Optical coherence tomography angiography (OCTA) is a novel noninvasive technology that provides depth-resolved visualization of the retinal and choroidal vasculature without the need for dye injection.[1–3] The technology relies on motion contrast to separate moving from stationary structures and to identify blood flow. This advanced imaging modality is as sensitive as dye-based angiography in detecting neovascularization in age-related macular degeneration (AMD) and provides more information about the extent and morphology of the neovascular (NV) lesion.[4] Several studies have characterized the detailed microvascular morphology of the three subtypes of NV lesions in AMD and have provided unprecedented structural detail of these abnormal vascular complexes.[5–7] Various anatomical descriptors, including "seafan," "medusa," "tangled," and "dead-tree" morphologies, have been used to characterize Type 1 neovascularization using OCTA analysis, whereas Type 3 lesions have been characterized as small vascular tufts.[7–12]

Despite these major technological advances that have provided incredible descriptive detail of the various forms of neovascularization in AMD, OCTA studies have failed to produce guidelines for treatment. Biomarkers of NV activity using OCTA analysis are

still lacking, and clinical practice continues to rely on structural OCT biomarkers of activity, including intraretinal and subretinal fluid.

Recent studies have used OCTA analysis to evaluate the morphologic characteristics of each subtype of neovascularization in AMD before and after treatment with anti–vascular endothelial growth factor (VEGF).[5,7,9,13,14] Other studies have found the sensitivity of OCTA in detecting NV lesions to range from 50% to 100%.[15–18] Liang et al[18] described a correlation of clinical activity versus the detection of neovascularization on OCTA but not versus the morphologic appearance. Many groups have observed the morphologic changes that occur after treatment at various intervals[19–21]; however, quantitative comparisons between different stages are still limited.

In this study, we performed qualitative and quantitative OCTA analyses of the structural features at baseline, after anti-VEGF treatment, and in eyes with clinically quiescent NV lesions.

Methods

This study was approved by the Institutional Review Board of the University of California, Los Angeles and conducted in accordance with the ethical standards stated in the Declaration of Helsinki. The study was conducted in accordance with the Health Insurance Portability and Accountability Act regulations. Written informed consent was obtained from all examined patients before OCTA imaging.

Study Population

Patients with Type 1 neovascularization secondary to AMD were enrolled in this study. A comprehensive chart review was performed to confirm the diagnosis and subtype of NV (Type 1, 2, or 3). The status of the disease was determined by a retina specialist (M.A., D. S.) on the basis of complete ophthalmologic examination and multimodal imaging, including fluorescein angiography (Heidelberg Engineering, Germany and Optos 200Tx; Optos, Scotland, United Kingdom) and structural OCT (Heidelberg Spectralis HRA + OCT; Heidelberg Engineering, Heidelberg, Germany).

All patients included in the study were at least 50 years of age, with AMD and Type 1 neovascularization associated with pigment epithelial detachment, as established using fluorescein angiography and spectral domain OCT at baseline diagnosis. Only those eyes with clear identification of the morphology and extent of the Type 1 neovascularization on OCTA (as determined by segmentation at the level of the choriocapillaris) were enrolled in this study. In addition, only lesions in which the entire extent of the lesions could be captured and measured were included in this study. The presence of any anatomical changes causing poor visualization of the NV membrane was an exclusion criterion. Intraretinal fluid and subretinal blood were not exclusion criteria as these abnormalities did not obstruct identification of the Type 1 NV lesion using OCTA. The cohort of eyes with AMD and Type 1 neovascularization was then divided into two groups: eyes with an active neovascularization lesion versus eyes with a quiescent lesion at the time of baseline examination. Clinical activity was defined similar to the retreatment criteria in the pro re nata arm of the HARBOR studies and included any evidence of disease activity on spectral domain OCT including presence of intraretinal fluid (i.e., intraretinal cysts, intraretinal edema, cystoid macular edema, retinal edema, retinal exudates, and intraretinal hemorrhage), the presence of subretinal fluid (i.e., serous retinal detachment, hemorrhagic retinal detachment, subretinal hemorrhage, and subretinal exudates), or presence of subretinal pigment epithelial fluid (i.e., hemorrhagic retinal pigment epithelium [RPE] detachment, sub-RPE hemorrhage).[22] A consecutive follow-up visit with repeat OCTA after treatment with anti-VEGF therapy and the absence of fluid and other activity signs on structural OCT were required for enrollment. For the group of patients with inactive or quiescent neovascularization, the requirements included a history of active Type 1 neovascularization treated with anti-VEGF at least 6 months prior and no signs of activity, either by clinical examination (i.e., subretinal hemorrhage) or by structural spectral domain OCT at the time of OCTA acquisition.

Image Acquisition and Analysis

The OCTA images were obtained using a spectral domain OCT device (RTVue-XR Avanti; Optovue, Inc,

From the *Doheny Image Reading Center, Doheny Eye Institute, Los Angeles, California; †Department of Ophthalmology, Stein Eye Institute, David Geffen School of Medicine at UCLA, Los Angeles, California; ‡Department of Ophthalmology, Faculty of Medicine Siriraj Hospital, Mahidol University, Bangkok, Thailand; and §Greater Los Angeles Veterans Affairs Healthcare System, Los Angeles, California.

D. Sarraf is a consultant and speaker for Optovue and consultant for Bayer and Genentech and receives research support from Allergan, Heidelberg, Regeneron, Genentech, and Optovue. S. R. Sadda is a consultant for Optos, Carl Zeiss Meditec, Allergan, Genentech, Regeneron, Bayer, Novartis, Iconic and receives research support from Optos, Carl Zeiss Meditec, Allergan, and Genentech. The remaining authors have no financial/conflicting interests to disclose.

Reprint requests: David Sarraf, MD, Retinal Disorders and Ophthalmic Genetics Division, Stein Eye Institute, UCLA, 100 Stein Plaza, Los Angeles, CA 90095; e-mail: dsarraf@ucla.edu

Fremont, CA) with split-spectrum amplitude decorrelation angiography algorithm.[3] The device operated with a central wavelength of 840 nm, an acquisition speed of 70,000 A-scans per second, and a bandwidth of 45 nm. The 3 mm × 3 mm scans were obtained with each cube consisting of 2 repeated volumes of 304 B-scans. Motion correction was performed using registration of the two orthogonally captured imaging volumes.[23,24] Automatic segmentation was performed by the viewing software to generate en face projection images of the NV lesion after adjusting the level of the segmented layer on the B-scans to best visualize the NV complex. Two horizontal segmentation lines contoured to the RPE profile were used to ensure a clear visualization of the NV complex located deep to the RPE.[25] In the event of segmentation errors, the thickness between the two segmentation lines was manually adjusted to include the whole NV complex. The upper line was located at the level of RPE to avoid a superimposition of the layers above. The lower line was moved progressively deeper toward the choroidal–scleral interface. This allowed visualization and analysis of all structures included in the choroidal en face slab. After each acquisition, the scans were reviewed for adequate image quality, motion artifacts, and extent of the NV membrane in relation to the field of view.

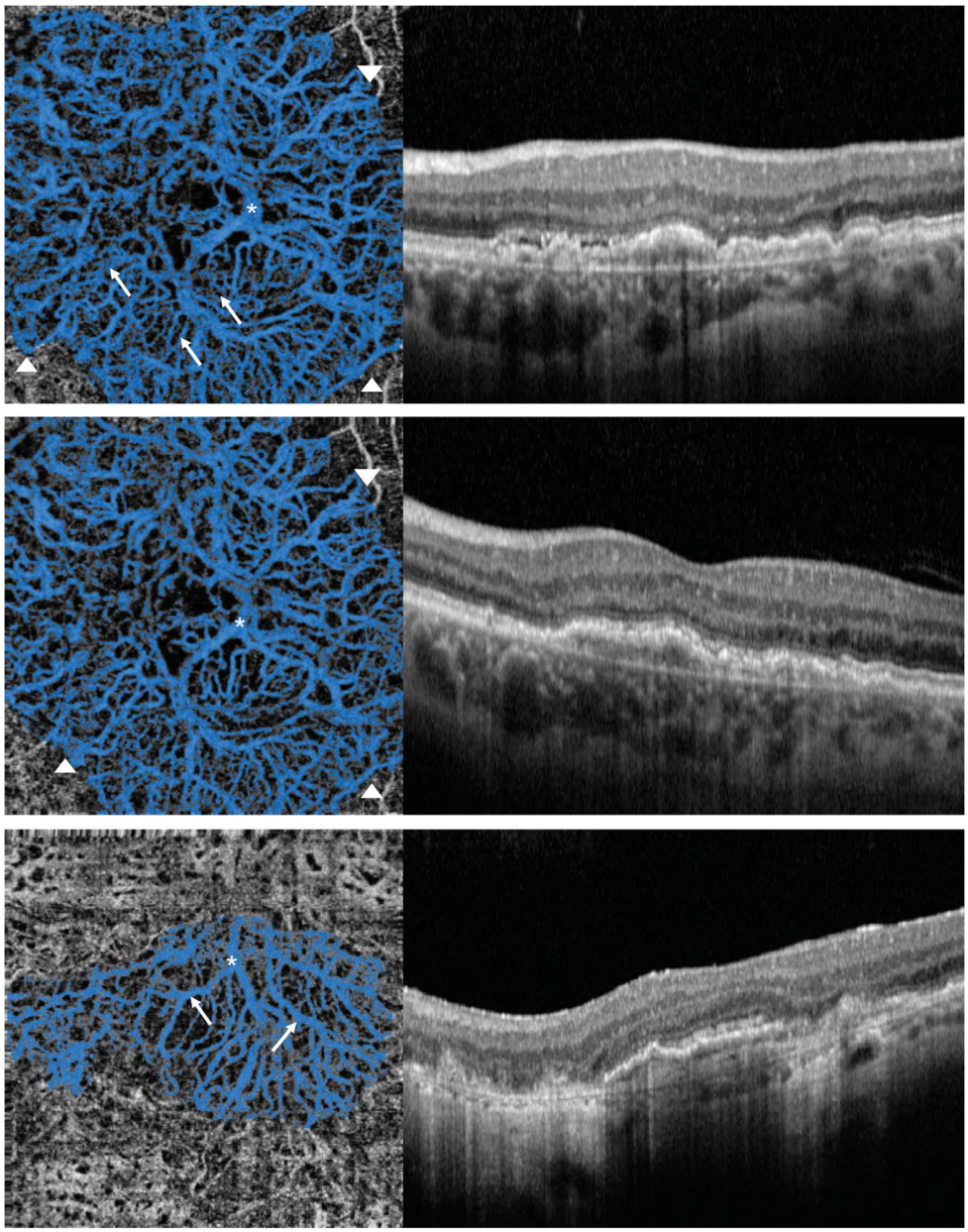

Fig. 1. Optical coherence tomography angiography characteristics to define morphologic features of neovascular lesions. (Upper images) Example of an active lesion, left eye of a 71-year-old man. (Upper left). Optical coherence tomography angiography en face projection image of the neovascular complex with vessels radiating in all directions from the center of the lesion. Note the presence of tiny vessels branching from bigger vessels (arrows), peripheral arcades at the vessel termini (arrow heads), and the prominent vessel (*). (Upper right) Corresponding spectral domain OCT B-scan. (Middle left) Follow-up OCTA 6 weeks later. Note the minimal change in the morphologic features and vessel density of the neovascular lesion after anti-VEGF therapy, although the finer vascular plexus appears to be attenuated. (Lower images) Example of a quiescent lesion, left eye of an 86-year-old female patient. Visual acuity was 20/30, status after 17 ranibizumab and 7 aflibercept injections, (last injection 15 months prior). (Lower left) Note the prominent vessel (*) and the dilated radiating vessels (arrows) and the absence of branching tiny vessels and absence of peripheral arcades of the vessel termini. Note that the radiating vessels are more dilated and demonstrate a straighter caliber.

Several anatomical features of the NV lesion were studied and included morphologic patterns such as a medusa or seafan pattern, branching with tiny vessels defined as fine anastomoses with numerous tiny radiating vessels branching from the center to the periphery, peripheral arcades defined as small anastomotic and looping vessels in the periphery branching into vascular arcades between the vessel termini, and presence of prominent central vessels. These features were analyzed on the en face images according to previous studies (Figure 1).[25] The NV lesion was divided into an inner segment (inner 80% of the lesion) and an outer fringe (outer 20% of the lesion) to quantitatively analyze the differences and evaluate the location of greatest activity (Figure 2). Quantitative OCTA analyses, including NV lesion area and vessel density, were performed using the publically available software ImageJ (public domain software; National Institutes of Health, Bethesda, MD).[26] The vessel density of the lesion was calculated as a ratio of the area occupied by vessels to the total area of the lesion. Pixel measurements were then calculated based on the 304-pixel width of the images. The measured area in pixels was converted to millimeters based on the scan dimensions (3 mm × 3 mm scan).

The fractal dimension (FD), a novel parameter used to evaluate neovascularization activity, enables

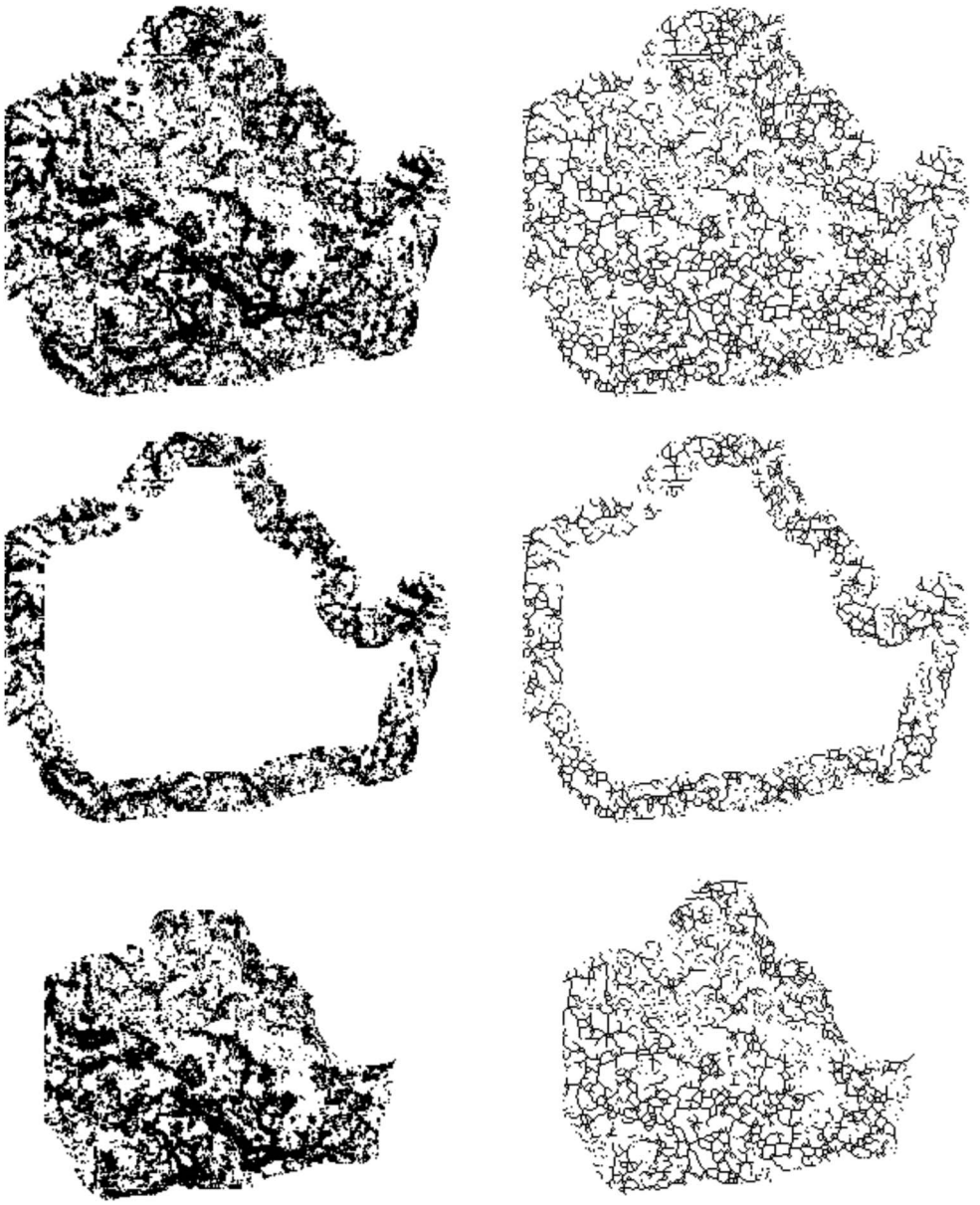

Fig. 2. Quantitative measurements of a neovascular lesion divided into its inner segment and outer fringe. (Left) Upper image demonstrates the total binarized neovascular lesion. Middle image demonstrates the outer fringe of the lesion (outer 20%) determined by measuring the dimensions of the lesion using ImageJ software and using the selection tools to shrink the border of the lesion by 20% while maintaining the shape. Lower image demonstrates the remaining 80% of the lesion (inner segment). (Right) Corresponding skeletonized images.

assessment of the architecture of a vascular network, particularly the degree of pattern complexity.[27,28] The FD was assessed using Fractalyse (ThéMA, Besançon Cedex, France) after the NV lesion was cropped, binarized, and skeletonized using ImageJ software. The FD analysis has been shown to be more sensitive when performed on skeletonized images versus binarized images.[29]

Fractalyse software measures the FD using the box-counting method.[30] The box-counting method consists of dividing a skeletonized image into square boxes of equal sizes and counting the number of boxes containing a vessel segment. The process is repeated several times with boxes of different sizes. The logarithm of the box size is plotted against the number of boxes containing a vessel segment using the following formula:

$$FD = \log(Ns)/\log(s).$$

In the equation, (Ns) is the number of boxes of magnification needed to enclose the structure, (s) is the size of the boxes. The FD varies with the distribution of skeletonized vessels of the image and has a value between 0 and 2 (Figure 3). The more complex the pattern, the higher the measured value.

All the measurements were made by two independent, masked readers (M.A. and N.A.I.). Disagreements over readings were resolved by open adjudication between readers.

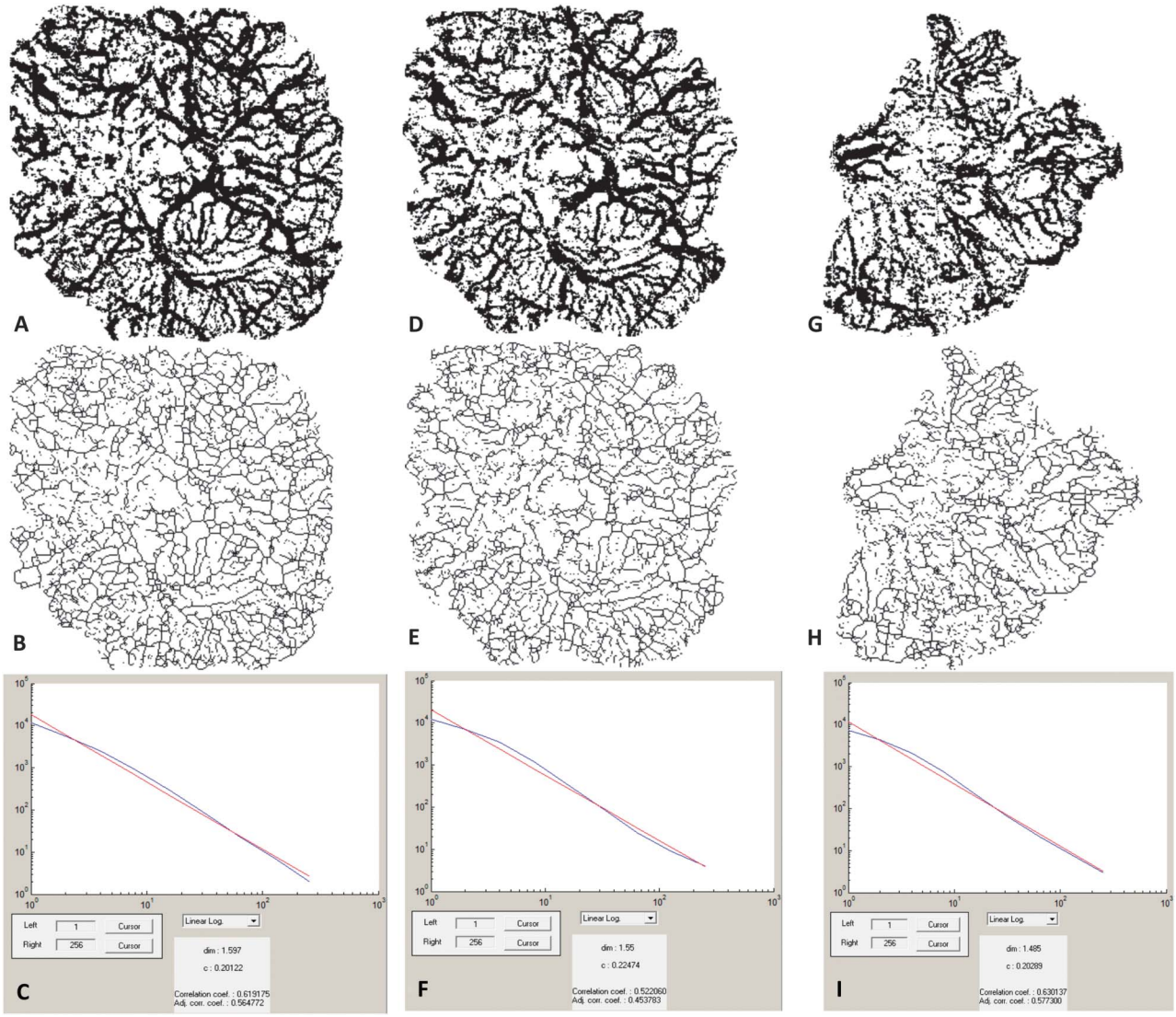

Fig. 3. Fractal dimension measurement (**A**) OCTA image of an active neovascular (NV) complex after cropping, binarization, and (**B**) skeletonization. **C.** Fractal analysis of the active NV lesion using the box-counting method of Fractalyse. **D–F.** Corresponding images (the same case as **A**) of the lesion after treatment with anti-VEGF therapy. **H–I.** Corresponding images of a quiescent NV lesion.

Statistical Analysis

Shapiro–Wilk test was used to evaluate the normal distribution. A paired samples *t* test was used to compare the patient group before and after treatment. An unpaired *t* test was used to compare the values to the second group with the quiescent neovascularization. Chi-square test was used to compare the categorical parameters. SPSS statistical software version 21 (SPSS Inc, IBM Company, Chicago, IL) was used for statistical analysis. A *P* value of <0.05 was considered significant.

Results

Thirty-one eyes from 21 patients were included in this study. Eleven eyes had active neovascularization at the baseline visit and were treated with anti-VEGF; 2 consecutive follow-up visits were evaluated in this study. Twenty eyes had quiescent neovascularization at the time of examination. The mean age in the group with active neovascularization was 80.8 years (range: 66–91); 7 were men and 4 were women. The mean number of intravitreal anti-VEGF injections received before the baseline visit was 14.4. The mean visual acuity at baseline was 20/50. The period between baseline and follow-up was 5.181 ± 1.250 weeks (range: 4–7 weeks). In the group with quiescent neovascularization, the mean age was 88.3 years (range: 76–96); 11 were women and 9 were men. The mean number of intravitreal anti-VEGF injections received before the baseline visit was 13.2. The mean visual acuity at the time of enrollment was 20/60. The mean duration of time since the last anti-VEGF injection was 10.5 months (range 6–36). There was no statistically significant difference between the two groups regarding age ($P = 0.365$), sex ($P = 0.545$), vision ($P = 0.667$), and number of injections at baseline ($P = 0.634$). Table 1 summarizes the baseline parameters.

Morphologically, of the patients with quiescent NV, eight had the previously described seafan pattern, five had the medusa pattern, and six were indistinct.[7] All the lesions had a prominent central vessel. Of those with active Type 1 lesions, two had the seafan pattern (2/2, 100% with prominent central vessel), five had the medusa pattern (4/5, 80% with prominent vessel), and four had indistinct patterns (1/4, 25% with prominent vessel).

Table 1. Baseline Parameters

	Active NV	Quiescent NV	*P*
Age	80.8	88.3	0.365
Sex			
Male/female	7/4	9/11	0.545
No. of injections	14.40	13.2	0.634
Visual acuity	20/50	20/60	0.667

NV, neovascular complex.

Of the 11 eyes with active NV lesions at baseline, 9 (81.81%) showed branching with numerous tiny vessels at baseline, and 7 (63.63%) showed similar morphologic changes in the follow-up visit after treatment with anti-VEGF ($P = 0.635$). Of the 20 eyes with quiescent neovascularization, 6 (30%) showed branching with tiny vessels ($P = 0.009$).

Of the 11 eyes with active neovascularization at baseline, 9 (81.81%) showed peripheral arcades. After treatmeant with anti-VEGF in all the 9 eyes the peripheral arcades were still visible ($P = 1$). Of the 20 eyes with a quiescent NV complex, 8 (40%) showed peripheral arcades at the vessel termini ($P = 0.057$). The branching vessels in the quiescent lesions showed a more dilated and straighter caliber and prominent anastomotic connections between large-diameter vessels. Figures 4 and 5 represent examples of active neovascularization lesion before and after treatment with anti-VEGF, and quiescent neovascularization lesions with the above-described morphologies.

The mean area of the lesion at baseline was 4.066 ± 2.838 mm^2 in the group with active neovascularization, 3.901 ± 3.130 mm^2 after treatment with anti-VEGF, and 3.503 ± 2.135 mm^2 in the group with quiescent NV. The vessel density of the lesion was 0.417 ± 0.044 in the group with active lesions before treatment, 0.412 ± 0.034 after treatment with anti-VEGF, and 0.433 ± 0.040 in the group of inactive or quiescent NV. No statistically significant difference was found in lesion area or vessel density between baseline and follow-up and quiescent lesions (lesion area $P = 0.43$, $P = 0.538$, $P = 0.211$; vessel density $P = 0.42$, $P = 0.35$, $P = 0.52$) for all eyes (Table 2).

The mean FD in the total area of the active lesion measured 1.57. The inner segment of the lesion measured 1.51, and the outer fringe measured 1.38. The FD in the total area of the lesion in eyes after treatment was 1.56, and was 1.47 in the inner segment of the lesion, and was 1.37 in the outer fringe of the lesion. Statistical significance when comparing the FD of active versus treated lesions was only noted about the inner segment of the lesion (*t* test for paired sample $P = 0.126$, $P = 0.048$, $P = 0.256$, Table 3).

The mean FD in eyes with quiescent NV was 1.44 in the total area, 1.35 in the inner segment, and 1.27 in the outer fringe. Comparing eyes with quiescent NV versus those with active NV, statistical significance was noted for all three respective parameters ($P = 0.009$, $P = 0.010$, and $P = 0.015$, Table 3).

Comparing the mean FD between the inner segment and outer fringe within a lesion, there was no statistically significant difference in the eyes with

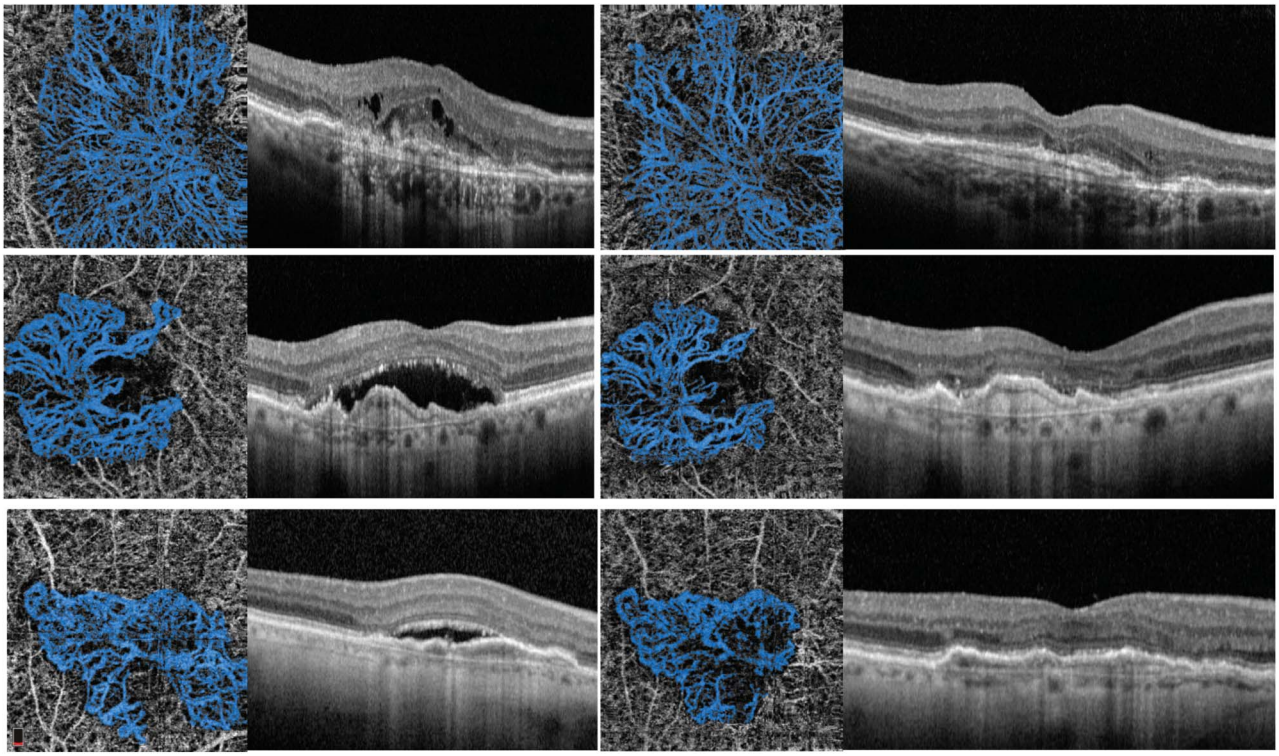

Fig. 4. Type 1 neovascularization in AMD before and after intravitreal anti-VEGF injections. (Upper images) The right eye of an 85-year-old female patient with visual acuity of 20/80 and status after 16 aflibercept injections. (Upper left) Optical coherence tomography angiography en face projection image of the neovascular complex with vessels radiating in all directions from the center of the lesion ("medusa pattern"). Note the radiating tiny vessels and the associated fibrovascular pigment epithelium detachment and cystoid macular edema on the structural B-scan OCT. (Upper right) Follow-up OCTA en face projection 5 weeks later with visual acuity of 20/70. Note the minimal change in vessel density and morphologic features of the neovascular lesion after anti-VEGF therapy, although the finer vascular plexus appears to be attenuated and the cystoid macular edema has resolved on the structural B-scan OCT. (Middle images) The right eye of a 78-year-old male patient with visual acuity of 20/60 and status after 3 aflibercept injections. (Middle left) Optical coherence tomography angiography en face projection image of the neovascular complex with vessels radiating from one side of the lesion (seafan pattern). Note the radiating tiny vessels and the peripheral arcades at vessel termini on OCTA as well as the associated fibrovascular pigment epithelium detachment and subretinal fluid on the structural B-scan OCT. (Middle right) Follow-up OCTA 6 weeks later with visual acuity of 20/60. Note the minimal change in vessel density and morphologic features after anti-VEGF therapy, although the finer vascular plexus appears to be attenuated and the subretinal fluid has resolved on the structural B-scan OCT. (Lower images) The right eye of an 89-year-old female patient with visual acuity of 20/40 and status after 10 aflibercept injections. (Lower left) Optical coherence tomography angiography en face projection image of the neovascular complex with vessels radiating in all directions from the center of the lesion (medusa pattern). Note the radiating tiny vessels and the peripheral arcades at vessel termini, and the associated fibrovascular pigment epithelium detachment and subretinal fluid on the structural B-scan OCT. (Lower right) Follow-up OCTA 6 weeks later with visual acuity of 20/40. Note the minimal change in vessel density and morphologic features after anti-VEGF therapy, although the finer vascular plexus appears to be attenuated and subretinal fluid has resolved on the structural B-scan OCT.

active NV, after receiving treatment, and those with quiescent NV ($P = 0.066$, $P = 0.148$, and $P = 0.65$).

Discussion

Optical coherence tomography angiography is a new imaging technology that provides more detailed microvascular morphologic information and greater quantitative capability of neovascular lesions in AMD versus conventional dye–based angiography.[4] In our study, we characterized and analyzed the NV complex qualitatively and quantitatively, comparing active NV lesions before and after treatment versus quiescent NV lesions secondary to AMD.

The morphologic appearance of Type 1 NV did not differ between the three groups, although there were a disproportionate number of seafan lesions in the quiescent group. This finding was consistent with a previous study describing a correlation between the presence of NV on OCTA and clinical activity but no correlation between the morphologic appearance of NV and clinical activity.[18]

A prominent central vessel was visible in all quiescent NV lesions in our study but was seen in only seven eyes (63.63%) with active NV. A prominent vessel was found more frequently in eyes with quiescent NV and is consistent with the maturity and chronicity of the lesion.[7,12] It has been hypothesized that these prominent vessels have different anatomical

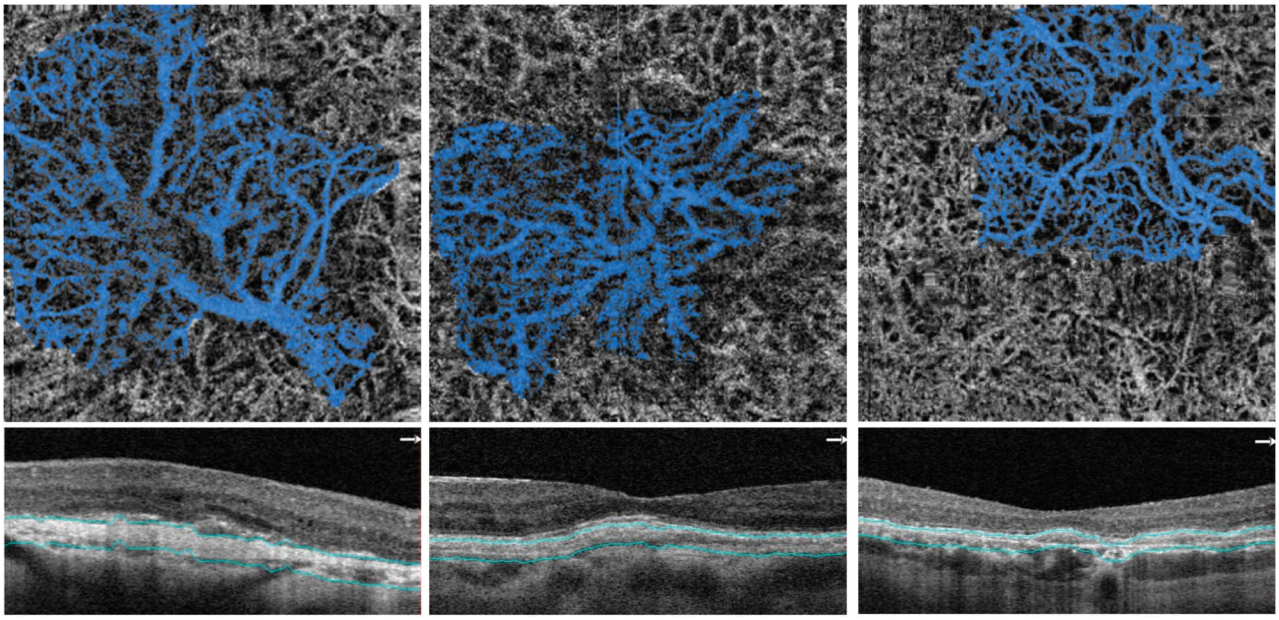

Fig. 5. Type 1 neovascularization in AMD in quiescent lesions. (Left) The right eye of an 86-year-old female patient with visual acuity of 20/50 and status after 17 ranibizumab injections (last injection 36 months prior). A 3 mm × 3 mm OCTA en face projection image of a quiescent neovascular (NV) complex with vessels radiating from one side of the lesion (seafan pattern). Note the prominent vessel and the dilated radiating vessels, and the absence of branching tiny vessels and absence of peripheral arcades of the vessel termini. Note that the radiating vessels are more dilated and demonstrate a straighter caliber; (below) corresponding SD OCT B-scan illustrating the corresponding segmentation. (Middle) Left eye of an 89-year-old female patient with visual acuity of 20/60 and status after 15 ranibizumab and 1 aflibercept injection (last injection 36 months prior). A 3 mm × 3 mm OCTA en face projection image of a quiescent NV complex with vessels radiating in all directions from the center of the lesion (medusa pattern). Note the prominent vessel and the dilated radiating vessels and the absence of branching tiny vessels and absence of peripheral arcades at the vessel termini; (below) corresponding segmentation B-scan. (Right) Left eye of an 80-year-old female patient with visual acuity of 20/60 and status after 9 aflibercept injections (last injection 14 months prior). A 3 mm × 3 mm OCTA en face projection image of a quiescent NV complex with vessels radiating in all directions from the center of the lesion (medusa pattern). Note the prominent vessel and the thick radiating vessels and the presence of branching tiny vessels but presence of few peripheral arcades at the vessel termini; (below) corresponding segmentation B-scan.

findings that make them more resistant to anti-VEGF therapy, including endothelial cells that are overlaid with protective pericytes, in contrast to the small caliber vessels made up of unprotected endothelial cells, which make them more responsive to treatment.[7,12,31,32]

Branching with tiny vessels was noted in 81.81% of active lesions and in 63.63% of the same eyes after

Table 2. Quantitative Measurement of the Lesion Area in mm^2, Vessel Density (Ratio), Vessel Density After Dividing Into Inner Segment and Outer Fringe in mm^2 at Baseline of Active Neovascular Lesions, After Treatment With Anti-VEGF, and Quiescent Lesions

	Active NV				
	Before Treatment	After Treatment	Quiescent NV	*P*	
Total lesion in mm^2	4.066 ± 2.838	3.901 ± 3.130	3.503 ± 2.135	Before vs. after treatment	0.433
				Active vs. quiescent	0.538
				After treatment vs. quiescent	0.211
Vessel density, ratio					
Total lesion	0.417 ± 0.044	0.412 ± 0.034	0.423 ± 0.040	Before vs. after treatment	0.426
				Active vs. quiescent	0.351
				After treatment vs. quiescent	0.528
Inner segment	0.427 ± 0.069	0.421 ± 0.054	0.421 ± 0.059	Before vs. after treatment	0.514
				Active vs. quiescent	0.884
				After treatment vs. quiescent	0.075
Outer fringe	0.414 ± 0.0315	0.408 ± 0.0360	0.439 ± 0.051	Before vs. after treatment	0.545
				Active vs. quiescent	0.102
				After treatment vs. quiescent	0.077

NV, neovascular complex.

Table 3. Fractal Dimension Measurements of the Active Neovascular Lesions, After Treatment With Anti-VEGF, and Quiescent Lesions Measured as a Total Area, Inner Segment, and Outer Fringe

	Active NV				
	Before Treatment	After Treatment	Quiescent NV	*P*	
Total lesion	1.574 ± 0.140	1.560 ± 0.155	1.446 ± 0.110	Before vs. after treatment	0.126
				Active vs. quiescent	0.009
Inner segment	1.516 ± 0.180	1.476 ± 0.171	1.351 ± 0.147	Before vs. after treatment	0.048
				Active vs. quiescent	0.010
Outer fringe	1.385 ± 0.127	1.374 ± 1.143	1.272 ± 0.111	Before vs. after treatment	0.256
				Active vs. quiescent	0.015

NV, neovascularization.

treatment with anti-VEGF; but these vessels were only noted in 30% of the quiescent NV lesions. This indicates that this morphologic finding may not differentiate active lesions before and after treatment but may aid in the identification of inactive or quiescent NV lesions. Similar findings were obtained with the analysis of peripheral arcades at the vessel termini. This potential biomarker may help differentiate an active versus a quiescent lesion but may not be as effective in guiding treatment and differentiating active NV lesions before and after treatment. Coscas et al[21] have previously identified these OCTA features as biomarkers of NV activity, but only in combination with other OCTA markers. As a single indicator, these features (e.g., peripheral arcades at the vessel termini) may not be sufficient to accurately judge activity.

We also found that the radiating vessels in quiescent lesions were more dilated and demonstrated a straighter caliber (Figures 1 and 5). This may be explained by the closure of the smaller vessels (containing unprotected endothelial cells), leading to increased vascular resistance of the entire NV complex as the remaining mature vessels (containing pericyte protected endothelial cells) develop higher intraluminal pressure and flow and, therefore, greater dilation of the vessel caliber.[7,12]

Lesion area and vessel density were compared between the 3 groups and no significant difference was identified, although quiescent lesions were on average 15% smaller in area than active lesions. Moreover, active lesions demonstrated minimal change after anti-VEGF therapy. Our findings are similar to those described by previous studies that demonstrated only subtle small vessel pruning after anti-VEGF therapy with subsequent vascular reproliferation or reperfusion as the NV lesion regains a morphology similar to its morphology before treatment.[7,12,15,19]

We used the novel parameter FD to study the complexity of the NV lesion. The FD measures the degree of pattern complexity with the box-counting method by dividing a skeletonized image into square boxes of equal sizes, where the number of boxes containing a vessel segment is counted. The FD has a value between 0 and 2 with higher values indicating increased pattern complexity. We found a reduced FD in the inner segment of the lesion when we compared eyes before and after treatment with anti-VEGF. Previous studies have noted that the core feeder and large-caliber vessels remain unchanged after anti-VEGF treatment, whereas the small-caliber vessels radiating from the larger trunks are attenuated and pruned.[7,12,13,19,20] Our finding of a reduced FD after treatment suggests that the pattern of the NV lesion after treatment might be less complex due to the attenuation and pruning of small-caliber vessels that may have a less significant effect on the vessel density compared with the large mature vessels.

Comparing eyes with active and quiescent NV, there was a statistically significant difference in the FD in the total or entire lesion complex and in the inner segment and outer fringe, suggesting that the vessels of a quiescent NV lesion show limited branching. Previous studies have noted that quiescent lesions may consist of larger, thicker, and straighter vessels.[20] We studied these changes quantitatively and found a reduced FD, meaning a less complex pattern of branching associated with quiescent NV (Figures 1 and 3).

Limitations of this study included the small sample size and the retrospective nature of the analysis with a lack of uniform follow-up periods. A limitation of the current OCTA technology is the accuracy of segmentation algorithms. Manual segmentation to more accurately locate the NV lesion was not possible, although the thickness of the segmentation slab was adjusted. Identification and inclusion of the entire NV complex can be challenging and is critical for accurate quantitative analysis. This may be further complicated by projection artifact that especially limits the accuracy of quantitation. Accurate repeatability of the segmentation parameters with follow-up can be

challenging because of changes in the anatomy that take place with treatment. Another limitation of the current technology was motion artifact that can especially disrupt quantitative measurements. As SSADA technology relies on the detection of motion of blood, any movement of the patient's head or eyes during image acquisition resulted in varying degrees of motion artifact and decreased image quality.

In summary, our study provides a comparative analysis of active NV before and after treatment, and versus quiescent Type 1 NV secondary to AMD. Qualitatively, quiescent NV demonstrated a lower incidence of branching of tiny vessels and peripheral arcades at vessel termini compared with active lesions, whereas inactive lesions (after treatment) did not differ morphologically from active lesions. These parameters may serve as anatomical biomarkers of activity and may help to differentiate an active lesion that requires therapy and/or close follow-up versus a quiescent lesion that does not need treatment and may be monitored less frequently. Using quantitative fractal analysis, NV lesion after treatment showed a reduced pattern complexity in the inner segment of the lesion compared with active NV, whereas quiescent NV showed reduced complexity in the total lesion area compared with active lesions before and after treatment. Quantitative fractal analysis of the branching pattern of NV may provide additional biomarkers to assess the activity of NV after anti-VEGF therapy and to determine the quiescent nature of lesions that do not require treatment. Future longitudinal studies with larger numbers of patients and standardized periods of follow-up are necessary to evaluate the morphologic and quantitative biomarkers of activity to better guide the treatment and monitoring of NV lesions in AMD and to more accurately assess the angiographic response.

In conclusion, OCTA is a new imaging modality that allows researchers to perform qualitative and quantitative analyses of NV lesions using a noninvasive technique with rapid acquisition. Analyzing the microvasculature complex and morphologic changes with OCTA may allow more precise monitoring of lesions during follow-up and after treatment with anti-VEGF, to better assess the efficacy of treatment and to more accurately evaluate the stage of the NV complex.

Key words: OCT angiography, quantitative analysis, fractal dimension, Type 1 neovascularization, active neovascularization, quiescent neovascularization, anti-VEGF.

References

1. Spaide RF, Klancnik JM Jr, Cooney MJ. Retinal vascular layers imaged by fluorescein angiography and optical coherence tomography angiography. JAMA Ophthalmol 2015;133:45–50.
2. Nagiel A, Sadda SR, Sarraf D. A promising future for optical coherence tomography angiography. JAMA Ophthalmol 2015;133:629–630.
3. Jia Y, Tan O, Tokayer J, et al. Split-spectrum amplitude-decorrelation angiography with optical coherence tomography. Opt Express 2012;20:4710–4725.
4. Inoue M, Jung JJ, Balaratnasingam C, et al. A comparison between optical coherence tomography angiography and fluorescein angiography for the imaging of Type 1 neovascularization. Invest Ophthalmol Vis Sci 2016;57:OCT314–OCT323.
5. Dansingani KK, Naysan J, Freund KB. En face oct angiography demonstrates flow in early Type 3 neovascularization (retinal angiomatous proliferation). Eye (Lond) 2015;29:703–706.
6. Iafe NA, Phasukkijwatana N, Sarraf D. Optical coherence tomography angiography of Type 1 neovascularization in age-related macular degeneration. Dev Ophthalmol 2016;56:45–51.
7. Kuehlewein L, Bansal M, Lenis TL, et al. Optical coherence tomography angiography of Type 1 neovascularization in age-related macular degeneration. Am J Ophthalmol 2015;160:739–748. e732.
8. Dansingani KK, Freund KB. Optical coherence tomography angiography reveals mature, tangled vascular networks in eyes with neovascular age-related macular degeneration showing resistance to geographic atrophy. Ophthalmic Surg Lasers Imaging Retina 2015;46:907–912.
9. Kuehlewein L, Dansingani KK, de Carlo TE, et al. Optical coherence tomography angiography of Type 3 neovascularization secondary to age-related macular degeneration. Retina 2015;35:2229–2235.
10. Miere A, Querques G, Semoun O, et al. Optical coherence tomography angiography in early Type 3 neovascularization. Retina 2015;35:2236–2241.
11. Miere A, Semoun O, Cohen SY, et al. Optical coherence tomography angiography features of subretinal fibrosis in age-related macular degeneration. Retina 2015;35:2275–2284.
12. Spaide RF. Optical coherence tomography angiography signs of vascular abnormalization with antiangiogenic therapy for choroidal neovascularization. Am J Ophthalmol 2015;160:6–16.
13. Coscas G, Lupidi M, Coscas F, et al. Optical coherence tomography angiography during follow-up: qualitative and quantitative analysis of mixed Type i and ii choroidal neovascularization after vascular endothelial growth factor trap therapy. Ophthalmic Res 2015;54:57–63.
14. Kuehlewein L, Sadda SR, Sarraf D. Oct angiography and sequential quantitative analysis of Type 2 neovascularization after ranibizumab therapy. Eye 2015;29:932–935.
15. de Carlo TE, Bonini Filho MA, Chin AT, et al. Spectral-domain optical coherence tomography angiography of choroidal neovascularization. Ophthalmology 2015;122:1228–1238.
16. Jia Y, Bailey ST, Wilson DJ, et al. Quantitative optical coherence tomography angiography of choroidal neovascularization in age-related macular degeneration. Ophthalmology 2014;121:1435–1444.
17. Moult E, Choi W, Waheed NK, et al. Ultrahigh-speed swept-source OCT angiography in exudative amd. Ophthalmic Surg Lasers Imaging Retina 2014;45:496–505.
18. Liang MC, de Carlo TE, Baumal CR, et al. Correlation of spectral domain optical coherence tomography angiography and clinical activity in neovascular age-related macular degeneration. Retina 2016;12:2265–2273.
19. Huang D, Jia Y, Rispoli M, et al. Optical coherence tomography angiography of time course of choroidal neovascularization

in response to anti-angiogenic treatment. Retina 2015;35: 2260–2264.
20. Lumbroso B, Rispoli M, Savastano MC. Longitudinal optical coherence tomography-angiography study of Type 2 naive choroidal neovascularization early response after treatment. Retina 2015;35:2242–2251.
21. Coscas GJ, Lupidi M, Coscas F, et al. Optical coherence tomography angiography versus traditional multimodal imaging in assessing the activity of exudative age-related macular degeneration: a new diagnostic challenge. Retina 2015;35: 2219–2228.
22. Busbee BG, Ho AC, Brown DM, et al. Twelve-month efficacy and safety of 0.5 mg or 2.0 mg ranibizumab in patients with subfoveal neovascular age-related macular degeneration. Ophthalmology 2013;120:1046–1056.
23. Kraus MF, Liu JJ, Schottenhamml J, et al. Quantitative 3d-oct motion correction with tilt and illumination correction, robust similarity measure and regularization. Biomed Opt Express 2014;5:2591–2613.
24. Kraus MF, Potsaid B, Mayer MA, et al. Motion correction in optical coherence tomography volumes on a per a-scan basis using orthogonal scan patterns. Biomed Opt Express 2012;3: 1182–1199.
25. Coscas F, Coscas G, Souied E, et al. Optical coherence tomography identification of occult choroidal neovascularization in age-related macular degeneration. Am J Ophthalmol 2007;144: 592–599.
26. Schneider CA, Rasband WS, Eliceiri KW. Nih image to imagej: 25 years of image analysis. Nat Methods 2012;9: 671–675.
27. Landini G, Murray PI, Misson GP. Local connected fractal dimensions and lacunarity analyses of 60 degrees fluorescein angiograms. Invest Ophthalmol Vis Sci 1995;36:2749–2755.
28. Reif R, Qin J, An L, et al. Quantifying optical microangiography images obtained from a spectral domain optical coherence tomography system. Int J Biomed Imaging 2012;2012: 509783.
29. Parsons-Wingerter P, Lwai B, Yang MC, et al. A novel assay of angiogenesis in the quail chorioallantoic membrane: stimulation by bfgf and inhibition by angiostatin according to fractal dimension and grid intersection. Microvasc Res 1998;55:201–214.
30. Masters BR. Fractal analysis of the vascular tree in the human retina. Annu Rev Biomed Eng 2004;6:427–452.
31. Bellou S, Pentheroudakis G, Murphy C, et al. Anti-angiogenesis in cancer therapy: hercules and hydra. Cancer Lett 2013; 338:219–228.
32. Benjamin LE, Hemo I, Keshet E. A plasticity window for blood vessel remodelling is defined by pericyte coverage of the preformed endothelial network and is regulated by pdgf-b and vegf. Development 1998;125:1591–1598.